How to cite: Angew. Chem. Int. Ed. 2023, e202306706
doi.org/10.1002/anie.202306706

Photoisomerization

Visible-Light-Triggered Photoswitching of Diphosphene Complexes

Clemens Taube[+], Jannis Fidelius[+], Kai Schwedtmann, Christopher Ziegler, Florian Kreuter, Leigh Loots, Leonard J. Barbour, Ralf Tonner-Zech, Robert Wolf,* and Jan J. Weigand**

In Memory of Edgar Niecke

Abstract: Although diphosphene transition metal complexes are known to undergo *E* to *Z* isomerization upon irradiation with UV light, their potential for photoswitching has remained poorly explored. In this study, we present diphosphene complexes capable of reversible photoisomerizations through haptotropic rearrangements. The compounds [(**2**-κ^2P,κ^6C)Mo(CO)$_2$][OTf] (**3a**[OTf]), [(**2**-κ^2P,κ^6C)Fe(CO)][OTf] (**3b**[OTf]), and [(**2**-κ^2P)Fe(CO)$_4$][OTf] (**4**[OTf]) were prepared using the triflate salt [(L$_C$)P=P(Dipp)][OTf] (**2**[OTf]) as a precursor (L$_C$ = 4,5-dichloro-1,3-bis(2,6-diisopropylphenyl)-imidazolin-2-yl; Dipp = 2,6-diisopropylphenyl, OTf = triflate). Upon exposure to blue or UV light (λ = 400 nm, 470 nm), the initially red-colored η^2-diphosphene complexes **3a**,**b**[OTf] readily undergo isomerization to form blue-colored η^1-complexes [(**2**-κ^1P,κ^6C)M(CO)$_n$][OTf] (**5a**,**b**[OTf]; **a**: M=Mo, n = 2; **b**: M=Fe, n = 1). This haptotropic rearrangement is reversible, and the (κ^2P,κ^6C)-coordination mode gradually reverts back upon dissolution in coordinating solvents or more rapidly upon exposure to yellow or red irradiation (λ = 590 nm, 630 nm). The electronic reasons for the reversible visible-light-induced photoswitching observed for **3a**,**b**[OTf] are elucidated by DFT calculations. These calculations indicate that the photochromic isomerization originates from the S$_1$ excited state and proceeds through a conical intersection.

Introduction

The dynamic molecular chemistry of photochromic molecules is of much interest because it potentially allows switching of physical and molecular properties through irradiation with (visible) light.[1] Photochromism finds practical utility across various domains such as functional molecular systems and chemical reaction networks, materials chemistry and the pharmaceutical sciences.[2] Many photoswitches capitalize on the inherent dynamic characteristics of organic molecules, e.g. the (*E*/*Z*)-isomerization of double bonds in alkenes and diazenes.[3] Diverse structural motifs can act as "photoactive" entities. Noteworthy examples encompass diazocines,[4] hydrazones,[5] and more recently documented indigoids[6] and Stenhouse dyes.[7]

Furthermore, the realm of photochromic properties extends to certain organometallic compounds, characterized by their propensity for haptotropic rearrangements, sigmatropic rearrangements, or linkage isomerism triggered upon irradiation.[8,9] Nonetheless, it is worth noting that the known photochromic organometallic molecules often exhibit limitations in their photoisomerization behavior, which typically falls under the thermal type (T type). In contrast, photochemical (P type) photoisomerization is less prevalent and primarily associated with processes necessitating UV irradiation.

Phosphaorganic ligands find extensive utility as hydrocarbon surrogates in coordination compounds and organometallic complexes.[10] In recent years, attention has been directed towards photoswitches, some of which incorporates a fusion of P-based ligands and transition metals,[11] while others focus purely on P moieties.[12] Notably, diphosphenes (RP=PR) represent a highly promising class of ligands.[13,14]

[*] Dr. C. Taube,[+] J. Fidelius,[+] Dr. K. Schwedtmann, Prof. Dr. J. J. Weigand
Faculty of Chemistry and Food Chemistry, Technische Universität Dresden, 01062 Dresden (Germany)
E-mail: jan.weigand@tu-dresden.de
Dr. C. Ziegler, Prof. Dr. R. Wolf
Institute of Inorganic Chemistry, Universität Regensburg, 93040 Regensburg (Germany)
E-mail: robert.wolf@chemie.uni-regensburg.de
F. Kreuter, Prof. Dr. R. Tonner-Zech
Wilhelm Ostwald Institute for Physical and Theoretical Chemistry, Universität Leipzig, 04103 Leipzig (Germany)
E-mail: ralf.tonner@uni-leipzig.de
Dr. L. Loots, Prof. Dr. L. J. Barbour, Prof. Dr. J. J. Weigand
Department of Chemistry and Polymer Science, Stellenbosch University, Stellenbosch 7602 (South Africa)
[+] These authors contributed equally to this work.

Despite this potential, exploration into the dynamic molecular chemistry of coordination compounds involving diphosphenes has been relatively limited. Surprisingly, even though the initial report on the photoisomerization of a transition metal diphosphene complex was published by Yoshifuji and co-workers as early as 1985,[15,16] comprehensive investigation remains scarce. A striking example involves the irradiation of (*E*)-configured Mes*P=P{M(CO)$_5$}Mes (*E*-**1**, Mes*=C$_6$H$_2$-2,4,6-(^{t}Bu)$_3$; M=Cr, Mo, W, Scheme 1, top) using a medium-pressure mercury lamp. The irradiation triggered the (*E*/*Z*)-photoisomerization of the P=P double bond, converting it to the corresponding (*Z*)-isomer *Z*-**1**. The (*Z*)-isomer, notably stable at ambient temperature, was successfully isolated through column chromatography and crystallization.

Reports of reversible isomerization to the (*E*)-isomer have not been documented. Similarly, certain uncomplexed (*E*)-diphosphenes undergo isomerization upon exposure to irradiation by a Laser[17] or a mercury lamp with Pyrex filter,[18] yielding mixtures of (*E*/*Z*)-isomers. In these cases, a thermal back-isomerization to the (*E*)-isomer was observed. It is noteworthy that precise control of the reaction temperature is required for such systems due to the potential occurrence of various side reactions, such as dimerization,[19] bond cleavage,[18] or non-selective proton shifts.[20] These undesirable processes can limit the efficiency and selectivity of the isomerization process.

In this context, we present the synthesis of new diphosphene complexes, namely [(**2**-κ^2P,κ^6C)Mo(CO)$_2$][OTf] (**3a**[OTf]), [(**2**-κ^2P,κ^6C)Fe(CO)][OTf] (**3b**[OTf]), and [(**2**-κ^2P)Fe(CO)$_4$][OTf] (**4**[OTf]) featuring the diphosphene cation [(L$_C$)P=P(Dipp)]$^+$ (**2**$^+$).[21–23] Significantly, we demonstrate the reversible photoswitching of **3a**,**b**[OTf] when subjected to visible light of various wavelengths. The electronic reasons for this photoisomerization process are elucidated by DFT calculations. This system represents a pioneering instance of photoswitching with phosphaorganometallic complexes, driven by visible light in both directions.

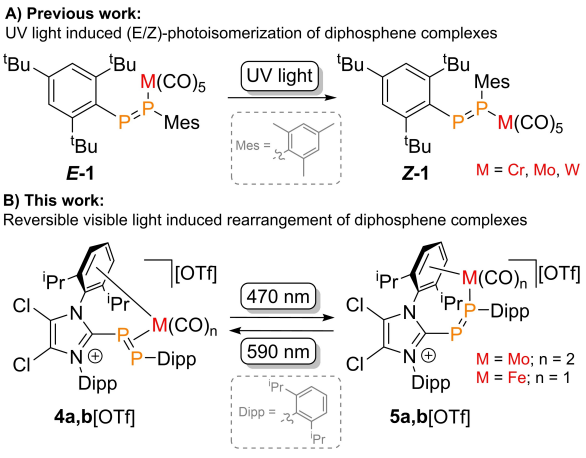

Scheme 1. Photoisomerization of diphosphene complexes.

Results and Discussion

Synthesis and Characterization of Cationic Diphosphene Complexes

In our pursuit of developing potentially photoactive new metal complexes, we reacted the recently reported diphosphene triflate salt [(L$_C$)P=P(Dipp)][OTf] (**2**[OTf]) with molybdenum carbonyl complex [Mo(CO)$_3$(CH$_3$CN)$_3$].[23] This reaction proceeds smoothly with the loss of one CO ligand and three molecules of CH$_3$CN. Following the work-up process, complex **3a**[OTf] is isolated as an air sensitive red solid with a yield of 58 %. The reaction of **2**[OTf] with [Fe$_2$(CO)$_9$] affords the yellow colored 1:1 complex **4**[OTf] with a yield of 75 % (Scheme 2). Complex **4**[OTf] was formed concomitantly with [Fe(CO)$_5$)] and contains a η^2-coordinated [Fe(CO)$_4$]-moiety. Both **3a**[OTf] and **4**[OTf] show well resolved AX spin systems in their ^{31}P NMR spectra (**3a**$^+$: $\delta(P_A) = -54.8$ ppm $\delta(P_X) = -9.0$ ppm, $^1J(P_AP_X) = -400$ Hz; **4**$^+$: $\delta(P_A) = -41.7$ ppm $\delta(P_X) = -8.8$ ppm, $^1J(P_AP_X) = -389$ Hz; Table 1), respectively. In comparison to the uncoordinated diphosphene **2**$^+$ (**2**$^+$: $\delta(P_A) = 398.1$ ppm $\delta(P_X) = 605.8$ ppm, $^1J(P_AP_X) = -577$ Hz; Table 1),[23] both complexes give rise to substantial high-field shifts and a reduced $^1J(P_AP_X)$ coupling constant due to electron transfer and the π-interaction of the P=P double bond with the low-valent metal centers.[13] The chemical

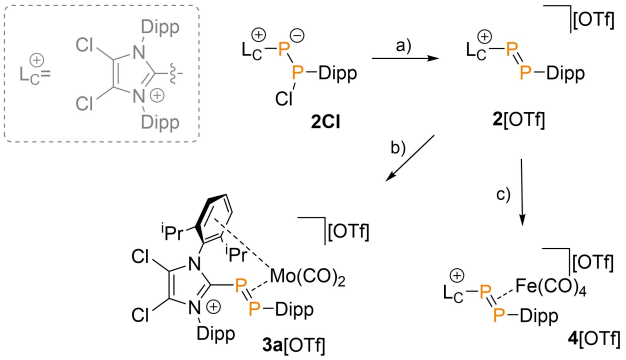

Scheme 2. Synthesis of cationic diphosphene [(L$_C$)P=P(Dipp)][OTf] (**2**[OTf]) from **2**Cl and subsequent synthesis of cationic and neutral diphosphene metal carbonyl complexes. Reagents and conditions: a) +Me$_3$SiOTf, −Me$_3$SiCl, PhF, 30 min, 86%; b) +[Mo(CO)$_3$(CH$_3$CN)$_3$], −CO, *o*-C$_6$H$_4$F$_2$, r.t., 16 h, 58%; c) +[Fe$_2$(CO)$_9$], −[Fe(CO)$_5$], CH$_2$Cl$_2$, r.t., 16 h, 75%.

Table 1: ^{31}P NMR data of the synthesized diphosphene complexes.

Complex	Solvent	$\delta(P_A)$ (in ppm)	$\delta(P_X)$ (in ppm)	$^1J(P_AP_X)$ (in Hz)
2Cl[22]	CD_2Cl_2	−13.7	133.8	−376
2[OTf][23]	CD_2Cl_2	398.1	605.8	−577
3a[OTf]	CD_2Cl_2	−54.8	−9.0	−400
3b[OTf]	thf-d_8	4.9	15.2	−345
4[OTf]	CD_3CN	−41.7	−8.8	−389
5a[OTf]	CD_2Cl_2	158.9	442.1	−468
5b[OTf]	CD_2Cl_2	124.1	353.3	−478

shifts of the P_X resonances are in line with those observed to related μ^3-(1κ^1P, 2κ^1P, 3κ^2P)-diphosphene complex such as [PhP=PPh(W(CO)$_5$)$_3$] ($\delta(P_X) = -16.6$ ppm).[24] The P_A resonances exhibits significant high-field shifts attributed to the influence of the imidazoliumyl substituent.

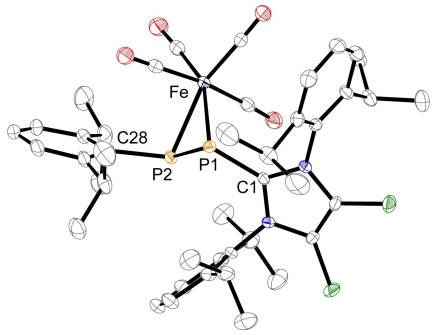

Figure 1. Molecular structure of **4**$^+$ in **4**[OTf]·3CH_2Cl_2; hydrogen atoms, solvate molecules and anion are omitted for clarity and thermal ellipsoids are displayed at 50% probability; selected bond lengths (Å) and angles (°) are listed in Table 2.

Single-crystal X-ray determinations confirmed the molecular structures (see Figure 1 for the structure of **4**[OTf], and Figure 2 for the structure of **3a**[OTf], and Table S1 for selected structural parameters). Notably, both structures display an η^2-coordinated diphosphene moiety (P–P 2.1352 (13) Å to 2.1594(12) Å).[13] Furthermore, complex **3a**[OTf] showcases an additional η^6-arene coordination of a Dipp substituent to the Mo atom. The C–C bond lengths of the η^6-coordinated arene ring (ranging from 1.388(6) Å to 1.435(5) Å) of **3a**[OTf] are slightly elongated compared to the second Dipp substituent (ranging from 1.377(7) Å to 1.404(6) Å). In line with these structural findings, the $^{13}C\{^1H\}$ NMR signals of the arene carbon atoms exhibit shifts toward higher field relative to the uncoordinated arene ring.[25]

The coordination of the diphosphene moiety to the transition metal carbonyl is also proven by IR spectroscopy, as evidenced by the CO stretching frequencies at 1925 cm^{-1} and 1981 cm^{-1} for complex **3a**[OTf]. Similarly, the IR stretching frequencies of the CO ligands in **4**[OTf] (2027 cm^{-1}, 2039 cm^{-1}, 2061 cm^{-1} and 2105 cm^{-1}) closely resembles those of the symmetrically diimidazoliumyl-substituted η^2-diphosphene complex [Fe(CO)$_4$(η^2-P$_2$(IMe$_4$)$_2$)][OTf]$_2$ (2048 cm^{-1}, 2074 cm^{-1} and 2116 cm^{-1}),[26] indicating

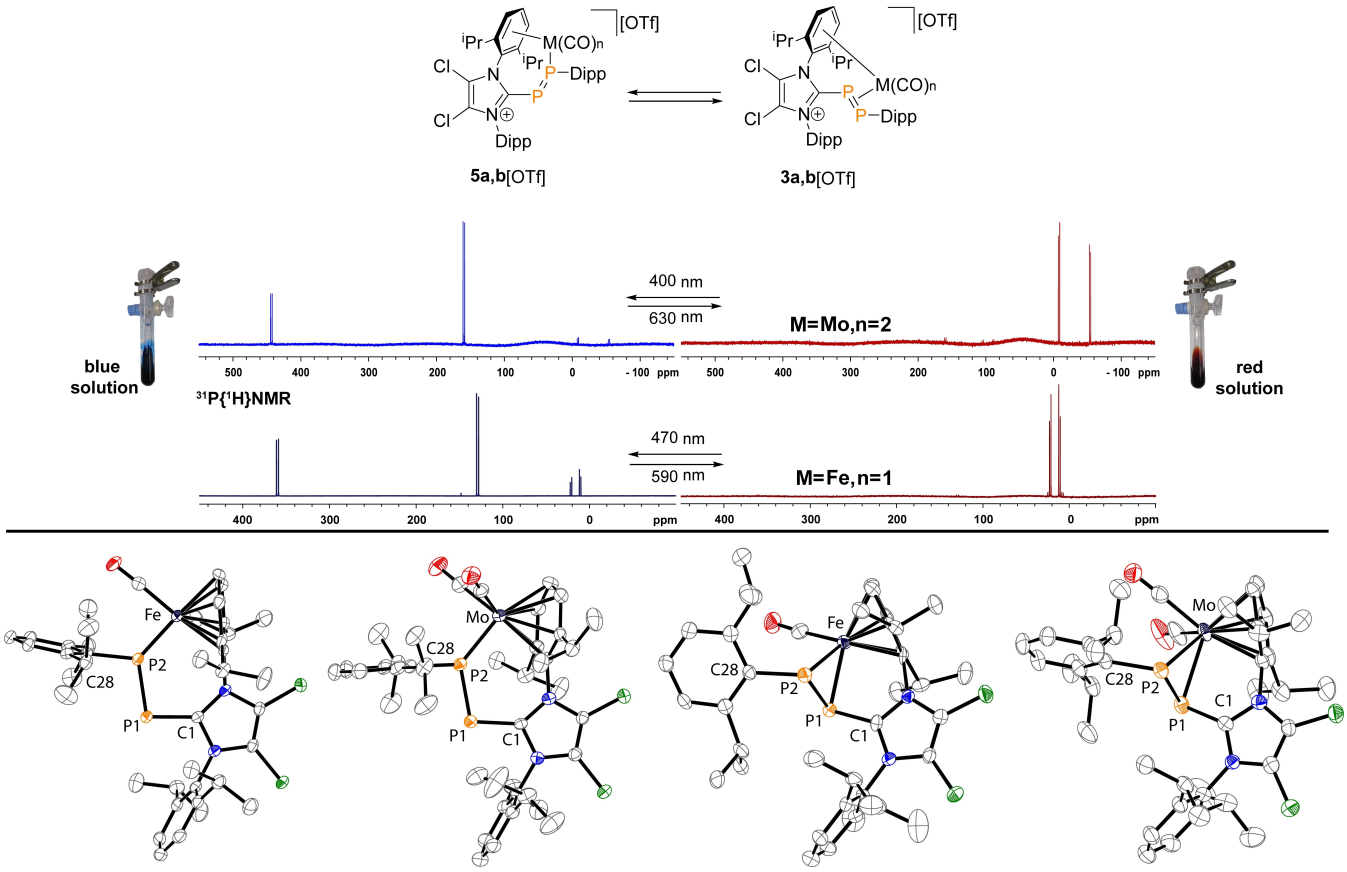

Figure 2. Graphical representation of the light-induced switching process between **3a**,**b**[OTf] and **5a**,**b**[OTf] (top) showing ^{31}P NMR spectra of the complexes and images of **5a**/**3a**[OTf] in solution (insets). The molecular structures of the diphosphene complexes are shown at the bottom (from left to right: **5b**$^+$ in **5b**[OTf]·THF, **5a**$^+$ in **5a**[OTf]·$MeNO_2$·0.75 Et_2O, **3b**$^+$ in **3b**[OTf]·PhF, and **3a**$^+$ in **3a**[OTf]·0.5 CH_2Cl_2); hydrogen atoms, solvate molecules and anions are omitted for clarity and thermal ellipsoids are displayed at 50% probability; selected bond lengths (Å) and angles (°) are listed in Table 2.

that the cationic diphosphene moiety in **4**[OTf] serves as a good π-acceptor in line with Tolman analysis.[27]

Investigation of the Photoisomerization Behavior of 3a[OTf] and 4[OTf]

A thorough investigation was conducted into the response of **3a**[OTf] and **4**[OTf] to irradiation by LEDs emitting at various wavelengths (λ_{max} = 365, 400, 470, 535 or 590 nm). Upon exposure to blue LED light (470 nm), the solution containing iron complex **4**[OTf] underwent a rapid transformation in color, transitioning from yellow to deep red-violet hue. Subsequently, complex **3b**[OTf] as the predominant product upon subjecting the crude mixture to stirring in THF overnight.

Structural characterization of **3b**[OTf] unveiled its status as the iron analogue of molybdenum complex **3a**[OTf], resulting from visible-light-induced decarbonylation (Scheme 3). The selective synthesis of **3b**[OTf] was accomplished through the utilization of a self-assembled flow reactor (detailed in Figure S16, SI), which enabled the isolation of air sensitive crystalline solid **3b**[OTf] in 57 % yield. This approach minimizes contact time, which is an important parameter due to the compound's susceptibility to degradation upon prolonged exposure to the blue LED light (see below). The ^{31}P NMR spectrum of isolated complex **3b**[OTf] exhibits the anticipated AX spin system (**3b**$^+$: $\delta(P_A)$ = 4.9 ppm $\delta(P_X)$ = 15.2 ppm, $^1J(P_AP_X)$ = −345 Hz Table 1) with low field shifted resonances along with a diminished $^1J(P_AP_X)$ coupling constant in comparison to **3a**[OTf]. This difference may arise from the increased back bonding interaction at the metal center.

In comparison to **4**[OTf], the IR stretching frequency of the CO ligand (1980 cm^{-1}) is shifted to lower wavenumbers, indicative of increased electron density at the metal center due to the substitution of three CO ligands by the arene ring. The structural parameters of **3b**$^+$ align closely with those of the molybdenum complex **3a**$^+$. The molecular structure of **3b**$^+$ (Figure 2) exhibits an η^2-coordinated diphosphene unit alongside an η^6-coordinated Dipp substituent.

Further exploration subjecting complexes **3a**,**b**[OTf] to irradiation by a blue LED (λ_{max} = 470 nm), resulting in discernible color transformation. Specifically, a shift from red to blue (**3a**$^+$ to **5a**$^+$) or from red to blue-violet (**3b**$^+$ to **5b**$^+$) was observed (Figure 2 and Supp. Video 1).

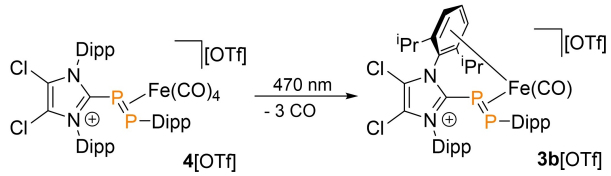

Scheme 3. Visible light induced decarbonylation of **4**[OTf] to **3b**[OTf]. Reagents and conditions: irradiation with blue LED (λ_{max} = 470 nm), PhF, flow reactor, 57 %.

The conversion of **3a**[OTf] to **5a**[OTf] proved notably swift, with a remarkable 91 % transformation observed within 3 min of irradiation, as deduced from the integration of the ^{31}P NMR resonances (Figure 3a, see the SI, section 3). Fine-tuning the excitation wavelength to 400 nm resulted in an impressive 96 % conversion of **3a**[OTf] to **5a**[OTf]. Notably, solid **3a**[OTf] can also be effectively transformed to **5a**[OTf] through blue light irradiation (Figure 2; see also section 3 of the SI). In contrast, the transition of **3b**[OTf] to **5b**[OTf] exhibits relatively slower kinetics, recording only 43 % conversion following 3 min of irradiation at 470 nm (Figure 3b), rising to 76 % after 12 min (see section 3 of the SI). As anticipated, employing a shorter irradiation time (90 s) yielded lower conversions (see Figure 3). Employing green (535 nm) or yellow light (590 nm), moderate conversion of 48 % and 8 % of **3a**[OTf], respectively, were achieved (Figure 3 and section 3, SI). Similar to **3b**[OTf], the synthesis of analytically pure **5b**[OTf] necessitated the application of the flow reactor due to decomposition upon prolonged irradiation with the blue light LED.

Compared to **3a**,**b**$^+$, the ^{31}P NMR spectra of complexes **5a**,**b**$^+$ exhibit strongly low-field shifted resonances for the AX spin system (**5a**$^+$: $\delta(P_A)$ = 158.9 ppm $\delta(P_X)$ = 442.1 ppm, $^1J(P_AP_X)$ = −468 Hz; **5b**$^+$: $\delta(P_A)$ = 124.1 ppm $\delta(P_X)$ = 353.3 ppm, $^1J(P_AP_X)$ = −478 Hz; Table 1), accompanied by increased magnitudes of the $^1J(P_AP_X)$ coupling constants

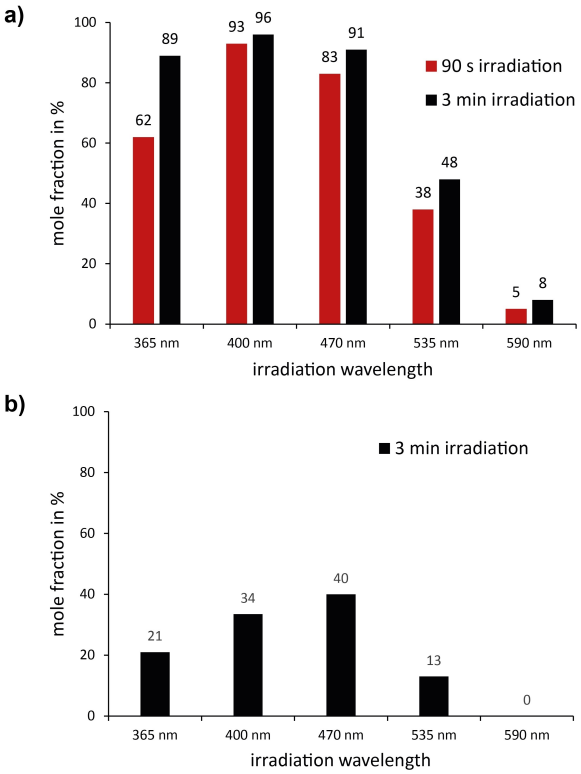

Figure 3. Conversion rates upon 3 min (black) or 90 s (red) of irradiation with different LEDs (λ_{max} = 365, 400, 470, 535 and 590 nm) for complexes **3a**[OTf] (a) and **3b**[OTf] (b); x-axis: wavelength of irradiating LED; y-axis: mole fraction of complex **5a**[OTf] (a) and **5b**[OTf] (b).

(Figure 2 and Table 1). Both observations collectively suggest an enhancement in the P=P double bond character, which further manifests itself in the shorter P=P bond lengths (see SI, Table S1). This data aligns well with *Yoshifuji's* diphosphene complexes, considering the acknowledged high-field shift of imidazoliumyl substituted P atoms (e.g. Mes*P=P{M(CO)$_5$}Mes (*E*-**1**, Scheme 1), $\delta(P_A) = 395.0$ ppm $\delta(P_X) = 486.3$ ppm, $^1J(P_AP_X) = -518$ Hz) for M=Mo).[15] Additionally, the IR stretching frequencies of the CO ligands (**5a**[OTf]: 1922 cm^{-1}, 1972 cm^{-1}; **5b**[OTf]: 1974 cm^{-1}) experience slight shifts towards lower wavenumbers when compared to **3a**,**b**[OTf], indicative of a relatively diminished electron transfer to the diphosphene moiety.

Validation of the molecular structure of cations **5a**,**b**$^+$ within **5a**,**b**[OTf] was achieved through X-ray analyses of crystals grown from $MeNO_2$/Et_2O (for **5a**[OTf]) and THF/*n*-pentane (of **5b**[OTf]). The X-ray crystallographic data, illustrated in Figure 2 and summarized in Table S1, confirm that both complexes exhibit a novel κ^1P^2-coordination for the diphosphene moiety, coupled with an additional η^6-coordination of one of the Dipp substituents at the Fe or Mo atoms. Consequently, **5a**,**b**[OTf] emerge as constitutional isomers of **3a**,**b**[OTf], a transformation attributed to a light-induced haptotropic rearrangement. Notably, the P=P bond lengths measuring 2.0816(15) Å (**5a**$^+$) and 2.0731(12) Å (**5b**$^+$) appear comparatively short in relation to **3a**,**b**[OTf] and correspond favorably with established η^1-diphosphene complexes.[15]

The C–P bond length likewise undergo a shortening, while the C–C bond lengths of the η^6-coordinated arene rings remain akin to those observed in **3a**,**b**[OTf]. A noteworthy observation pertains to the Dipp substituent on the diphosphene moiety, which undergoes an approximate 90° rotation upon excitation in both complexes. This behavior can be attributed to the pronounced alteration in steric demand imposed by the P–M coordination.

In our attempts to isolate **5a**,**b**[OTf], the samples consistently exhibited minor contamination with **3a**,**b**[OTf], despite numerous attempts to seperate the species through intricate purification procedures. The consistent occurrence of such contamination indicated the reversibility of the isomerization process. Subsequent ^{31}P NMR investigations suggest that **5a**,**b**[OTf] re-isomerizes to **3a**,**b**[OTf] in the absence of irradiation, even at room temperature in THF. Over a span of 16 h, the integration of resonances within the ^{31}P NMR spectra illustrated conversions of approximately 81 % for **3a**$^+$ and 90 % **3b**$^+$ in THF. To gain a deeper understanding of the kinetics, we conducted studies to estimate the activation barrier of the reverse reaction by temperature dependent NMR investigations (see SI, section 3). Our findings reveal that the activation energy for the conversion of **5a**[OTf] to **3a**[OTf] (92.7 kJ/mol) surpasses that for the transformation of **5b**[OTf] to **3b**[OTf] (76.4 kJ/mol) by 16.3 kJ/mol. It seems important to note that the reverse reaction of **5b**[OTf] also occurs in non-coordinating solvents like CH_2Cl_2, while **5a**[OTf] remains stable under similar conditions.

The UV/Vis spectra of **5a**,**b**[OTf] reveal absorption maxima (**5a**$^+$: 624 nm; **5b**$^+$: 569 nm) displaying a hypsochromic shift when contrasted with **3a**,**b**[OTf] (**3a**$^+$: 353 nm; **3b**$^+$: 382 nm). This pronounced shift indicates positive photochromism, inciting our investigation into the rate of the reverse reaction (**5a**,**b**[OTf] to **3a**,**b**[OTf]) upon irradiation with LED ($\lambda_{max} = 630$ nm). These reactions were conducted by ^{31}P NMR monitoring at low temperatures (−30 °C) to exclude thermally induced back reaction. Significantly, within 15 min of irradiation, complete conversion was accomplished for **5a**[OTf] (see the SI, section 3). Under analogous conditions, a 3-min irradiation period yielded 79 % conversion for **5b**[OTf] (see section 3 of the SI). It is important to note that during red light irradiation, partial decomposition of **5b**[OTf] was observed. Similarly, both reactions were replicated with yellow light irradiation ($\lambda_{max} = 590$ nm) at room temperature, resulting in comparatively lower conversion rates. Of note, **3a**[OTf] demonstrated photostability, capable of undergoing ten cycles without appreciable decomposition. In contrast, **3b**[OTf] exhibited partial degradation after three cycles.

In summary, the transformation of **3a**,**b**[OTf] to **5a**,**b**[OTf] in solution is appropriately classified as a thermally and photochemically reversible photochromic process of both types T and P.[9]

Furthermore, our exploration extended to investigating these switching reactions in solid state (see SI, section S3). Initially, the switching process was monitored by IR spectroscopy. Our findings revealed that both complexes **3a**,**b**[OTf] can undergo the excitation reaction to form **5a**,**b**[OTf]. To examine the reverse reaction, both complexes were subjected to either red light or heating (60 °C). Interestingly, **5a**[OTf] could be selectively converted back to **3a**[OTf] through irradiation with red light, while heating did not facilitate the same reversion. Similarly, the iron complex **3b**[OTf] could be excited to yield **5b**[OTf]. However, the reverse reaction was not observed when the sample was heated or exposed to red light. To further support the IR observations, **3a**[OTf] was subjected to differential scanning photo-calorimetry (photo-DSC; see SI, section S3). The measurements were carried out using a custom-built hermetic sample compartment, which enabled sample irradiation under isothermal conditions. The photo-DSC results recorded at both 0 and 40 °C are consistent with the conversion of **3a**[OTf] to **5a**[OTf] upon 400 nm irradiation, and the reversion of **5a**[OTf] to **3a**[OTf] when exposed to 640 nm light. After the irradiation events, conventional DSC showed no thermal event occurring upon heating to 100 °C. Interconversion between **3a**[OTf] and **5a**[OTf] could not be supported by powder X-ray diffraction analysis (see SI, section S3), possibly owing to insignificant structural changes due to isomerization, as well as amorphization of the sample upon irradiation.

Quantum Chemical Calculations

We set out with theoretical studies to understand molecular excitations accountable for the photochemical transition

between **3a**,**b**$^+$ and **5a**,**b**$^+$. To this end, the absorption spectra were initially computed using TD-DFT (ωB97X-D3/def2-TZVP) to validate the accuracy of our computational approach. The method employed, along with the simulated spectra, is further described in the SI. This chosen approach closely reproduces the experimental spectra, displaying a constant and minor shift of less than 40 nm (see Figures S67–S70, SI). In exploring the potential energy surfaces of the excited state, we opted for model systems (**3a′**, **3b′**, **5a′**, **5b′**) in which the isopropyl groups are substituted by hydrogen atoms (here the '+' is omitted in this section to signify that the influence of the anion is disregarded in the computations). The utilization of these model compounds subtly influences the atomic configurations but negligibly affects electronic properties when the arrangement of phenyl groups is confined to match the observed arrangement in the molecular structures of **3a**,**b**$^+$ and **5a**,**b**$^+$ (see the Table S1). Upon optimizing structures of the ten lowest-lying excited states, we identified a barrierless reaction for the first excited state in both forward and backward reactions of both Fe- and Mo-complexes (Figure 4), respectively. That implies that optimization from the vertically excited state results in structural changes towards the product, bringing the energy levels of the ground state and first excited state closer together (Figure 4a and 4b). Interestingly, for all other investigated excited states, minimal structural changes were observed upon optimization, affirming the experimental observation that these complexes can be excited by light and readily proceed to the desired products without barriers. As we traced the reaction coordinate, a point of near-degeneracy between the ground and excited state emerged after a certain number of optimization steps (Figure 4a: structure **Mo-I** in reaction **3a′***→**5a′**; Figure 4b: structure **Mo-IV** in reaction **5a′***→**3a′**; the asterisk signifies an electronically excited state). At these junctures, optimization halts due to a negative eigenvalue in the excited state calculation, indicating an energetical inversion where the ground state surpasses the excited state. This signifies a conical intersection. Characteristic structural changes are associated with the reaction. In the forward reaction (Figure 4a: **3a′***→**5a′**), the Mo–P1-P2 bond angle shifts from 66.3° (**3a′***) to 85.8° (**Mo-I**) and culminates at 128.3° in product **5a**$^+$. Furthermore, the Mo–P1/2 distances diverge, signifying a shift from η^2-coordination of **3a′** to η^1-coordination in **5a′**. In contrast, the backward reaction (Figure 4b: **5a′***→**3a′**) exhibits an inversely proportional trend in Mo–P1–P2 bond angle, progressing from 128.3° (**5a′***) through 103.5° (**Mo-IV**) and returning to 66.3° (**3a′**). To demonstrate that these excited state optimizations indeed yield the desired products, structures **Mo-I** and **Mo-IV** were slightly distorted in the products' direction, adjusting from 85.8° to 90.3° for the forward reaction and from 103.5° to 101.0° for the backward reaction. Subsequent ground state optimizations were performed. The resulting energy curves are displayed on the right-hand side of Figures 4a and 4b. This analysis conclusively establishes that once the conical intersection is traversed, the structures undergo barrierless optimization into the desired products.

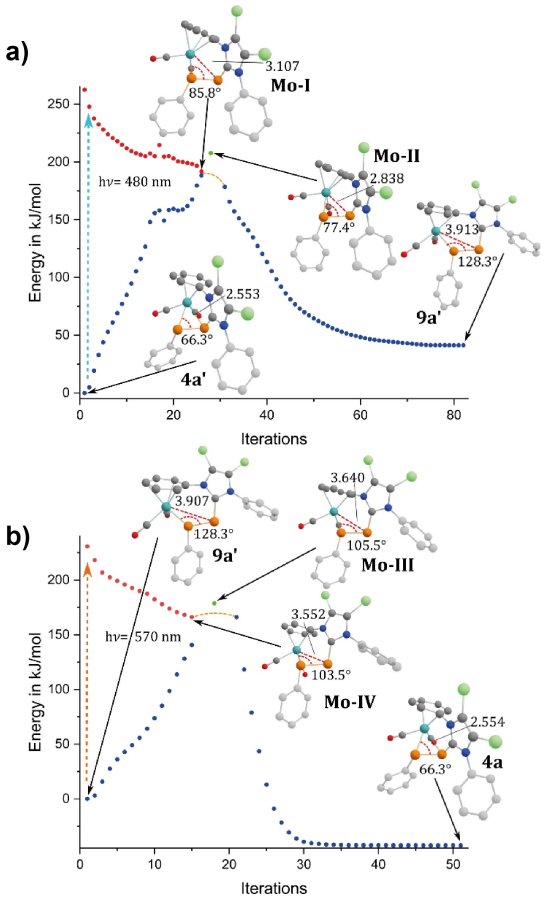

Figure 4. Energy profile of the Mo complex for the a) forward reaction **3a′*** to **5a′** and b) the backward reaction **5a′*** to **3a′** with energies from ground state calculations (blue), energies of the first excited state (red) and the separately optimized conical intersection structures **Mo-II**, **Mo-III** (green). The structures up to the points **Mo-I** and **Mo-IV** stem from excited state optimizations while ground state optimizations were conducted after the conical intersections. In between these two regimes, the structure had to be slightly manually distorted due to the inadequacy of TD-DFT to describe the multireference character of the complexes here (orange dashed lines). All distances are given in Å.

Given that excited state optimizations cease at the structures **Mo-I** and **Mo-IV**, we conducted separate optimization for the conical intersection structures. These are illustrated in Figures 4a (**Mo-II**) and 4b (**Mo-III**) for the forward and backward reaction, respectively. Despite slight deviations in energy and structure, **Mo-II** and **Mo-III** bear strong resemblance to structures **Mo-I** and **Mo-IV**, underscoring the accuracy of our approach in estimating conical intersection structures. Notably, both structures consistently mirror the hapticity changes observed in the aforementioned experimental structures.

Our examination of the iron complex yields analogous findings (see Figure S75). For both forward and backward reaction, the first excited state is responsible. Due to convergence challenges, full convergence for the forward reaction of the iron complex could not be achieved.

To summarize, our calculations compellingly indicate that the first excited state drives the photochemical trans-

Table 2: Uncorrected ΔE_{cal} and corrected ΔE_{cal}^{corr} computed (ωB97X-D3/def2-TZVP) first excitation energy in comparison to experimentally used wavelengths ΔE_{exp}.

Complex	ΔE_{cal} [nm]	ΔE_{cal}^{corr} [nm]	ΔE_{exp}
3a′	474.4	480	470
3b′	480.1	500	470
5a′	568.9	590	
5b′	594.4	640	

formation in the hapticity of the diphosphene complexes $\mathbf{3a}^+$ and $\mathbf{3b}^+$. Furthermore, it is noteworthy that the theoretical results closely align with the experimentally employed excitation wavelength (Table 2), with the computed excitation energies being corrected to account for the energy difference between the lowest and highest peak in respective experimental and calculated spectra (Figures S67–S70, SI). This correction facilitates the calculation of the average shift in calculated excitation energy.

Conclusion

In summary, both the diphosphanide (L_C)P–P(Cl)(Dipp) (**2**Cl) and the cationic diphosphene triflate salt [(L_C)P=P(Dipp)][OTf] (**2**[OTf]) serve as effective precursors for the generation of transition metal carbonyl η^2-diphosphene complexes **3a**[OTf], [(**2**-κ^2P,κ^6C)Mo(CO)$_2$][OTf] and **3b**[OTf] [(**2**-κ^2P,κ^6C)Fe(CO)][OTf], with the latter arising from the visible light induced decarbonylation of **4**[OTf] [(**2**-κ^2P)Fe(CO)$_4$][OTf]. Of particular note, complexes **3a**,**b**[OTf] exhibit remarkable photochromic properties, a consequence of light-induced haptotropic rearrangement, leading to the conversion **3a**,**b**[OTf] to η^1-diphosphene isomers **5a**,**b**[OTf]. This intriguing process is reversible through either thermal treatment or photochemical stimulation by yellow/red LED light (590/630 nm). It is worth highlighting that the solid state investigations reveal differing behavior for **3a**,**b**[OTf]. While **3a**[OTf] can be switched back and forth photochemically, **3b**[OTf] can be excited to **5b**[OTf] but does not revert back to **3b**[OTf]. Additionally, both **5a**,**b**[OTf] demonstrate stability at elevated temperatures in solid state. Theoretical investigations unveil that the photochromic behavior finds its origins in the S_1 excited state for both forward and reverse reaction. Moreover, the photochemical switching from **3a**,**b**[OTf] to **5a**,**b**[OTf] proceeds through a conical intersection, rendering **5a**,**b**-[OTf] relatively inert. Considering the established role of organometallic compounds as photochromic switches, our findings indicate that overlooked diphosphene complexes exhibit significant promise in the field of photochromic properties. Future research efforts will concentrate on harnessing and refining this behavior to further enhance the photochemical characteristics.

Acknowledgements

We gratefully acknowledge the support provided by the German Research Foundation (DFG) through grant numbers WE4621/3-1, WE4621/3-2; WE 4621/6-1; WO1496/7-1, and WO1496/7-2, as well as the support from the Research Training Group GRK1782. We extend our appreciation to GOETHE-CSC Frankfurt for providing computational resources. J.F. expresses gratitude to the Graduate Academy of the TU Dresden for financial assistance provided. Philipp Lange is acknowledged for performing elemental analyses. Financial support from TUD is also acknowledged and greatly appreciated. Open Access funding enabled and organized by Projekt DEAL.

Conflict of Interest

The authors declare no conflict of interest.

Data Availability Statement

The data that support the findings of this study are available in the supplementary material of this article. Deposition numbers 2237447 (for **3a**[OTf]), 2237448 (for **3b**[OTf]), 2237449 (for **4**[OTf]), 2237453 (for **5a**[OTf]), and 2237454 (for **5b**[OTf]) contain the supplementary crystallographic data for this paper. These data are provided free of charge by the joint Cambridge Crystallographic Data Centre and Fachinformationszentrum Karlsruhe Access Structures service. Data regarding the DFT calculations can be accessed from the NOMAD database under https://dx.doi.org/10.17172/NOMAD/2023.01.20-2.

Keywords: Diphosphenes · Photoisomerization · Photoswitch · Quantum Chemical Calculations · Structure Elucidation

[1] a) Z. L. Pianowski, *Molecular Photoswitches*, Wiley **2022**; b) B. L. Feringa, W. R. Browne, *Molecular switches*, Wiley-VCH, Weinheim **2011**; c) A. S. Lubbe, T. van Leeuwen, S. J. Wezenberg, B. L. Feringa, *Tetrahedron* **2017**, *73*, 4837.
[2] a) A. Goulet-Hanssens, F. Eisenreich, S. Hecht, *Adv. Mater.* **2020**, *32*, e1905966; b) J. Volarić, W. Szymanski, N. A. Simeth, B. L. Feringa, *Chem. Soc. Rev.* **2021**, *50*, 12377; c) Z. Zhang, W. Wang, M. O'Hagan, J. Dai, J. Zhang, H. Tian, *Angew. Chem. Int. Ed.* **2022**, *61*, e202205758.
[3] a) D. Cameron, S. Eisler, *J. Phys. Org. Chem.* **2018**, *31*, e3858; b) R. F. Tabor, T. M. McCoy, Y. Hu, B. L. Wilkinson, *Bull. Chem. Soc. Jpn.* **2018**, *91*, 932; c) R. Dorel, B. L. Feringa, *Chem. Commun.* **2019**, *55*, 6477; d) D. Villarón, S. J. Wezenberg, *Angew. Chem. Int. Ed.* **2020**, *59*, 13192; e) S. Crespi, N. A. Simeth, B. König, *Nat. Chem. Rev.* **2019**, *3*, 133.
[4] M. Hammerich, C. Schütt, C. Stähler, P. Lentes, F. Röhricht, R. Höppner, R. Herges, *J. Am. Chem. Soc.* **2016**, *138*, 13111.
[5] B. Shao, I. Aprahamian, *Chem* **2020**, *6*, 2162.
[6] C. Petermayer, H. Dube, *Acc. Chem. Res.* **2018**, *51*, 1153.
[7] S. Helmy, S. Oh, F. A. Leibfarth, C. J. Hawker, J. Read de Alaniz, *J. Org. Chem.* **2014**, *79*, 11316.

[8] a) H. Maeda, M. Nishikawa, R. Sakamoto, H. Nishihara, *Comprehensive Inorganic Chemistry III*, Elsevier, Amsterdam **2023**, pp. 356–416; b) S. Niibayashi, K. Matsubara, M. Haga, H. Nagashima, *Organometallics* **2004**, *23*, 635; c) H. Nagashima, T. Fukahori, M. Nobata, A. Suzuki, M. Nakazawa, K. Itoh, *Organometallics* **1994**, *13*, 3427; d) I. D. Gridnev, *Coord. Chem. Rev.* **2008**, *252*, 1798; e) A. Y. Kovalevsky, K. A. Bagley, J. M. Cole, P. Coppens, *Inorg. Chem.* **2003**, *42*, 140; f) K. A. Deresz, R. Kamiński, S. E. Kutniewska, A. Krówczyński, D. Schaniel, K. N. Jarzembska, *Chem. Commun.* **2022**, *58*, 13439; g) G. C. Thaggard, J. Haimerl, K. C. Park, J. Lim, R. A. Fischer, B. K. P. Maldeni Kankanamalage, B. J. Yarbrough, G. R. Wilson, N. B. Shustova, *J. Am. Chem. Soc.* **2022**, *144*, 23249; h) M. Slota, M. Blankenhorn, E. Heintze, M. Vu, R. Hübner, L. Bogani, *Faraday Discuss.* **2015**, *185*, 347.
[9] H. Nakai, K. Isobe, *Coord. Chem. Rev.* **2010**, *254*, 2652.
[10] a) K. B. Dillon, F. Mathey, J. F. Nixon, *Phosphorus, the carbon copy. From organophosphorus to phospha-organic chemistry*, Wiley, New York **1998**; b) F. Mathey, *Angew. Chem. Int. Ed.* **2003**, *42*, 1578.
[11] a) H. Ube, Y. Yasuda, H. Sato, M. Shionoya, *Nat. Commun.* **2017**, *8*, 14296; b) F. Beltran, E. Bergamaschi, I. Funes-Ardoiz, C. J. Teskey, *Angew. Chem. Int. Ed. Engl.* **2020**, *59*, 21176; c) D. Lunic, E. Bergamaschi, C. J. Teskey, *Angew. Chem. Int. Ed. Engl.* **2021**, *60*, 20594.
[12] a) J. Bresien, T. Kröger-Badge, S. Lochbrunner, D. Michalik, H. Müller, A. Schulz, E. Zander, *Chem. Sci.* **2019**, *10*, 3486; b) F. Buß, M. Das, D. Jannsen-Müller, A. Sietmann, A. Das, L. F. B. Wilm, M. Freitag, M. Seidl, F. Glorius, F. Dielmann, *Chem. Commun.* **2023**, *59*, 12019.
[13] L. Weber, *Chem. Rev.* **1992**, *92*, 1839.
[14] M. Yoshifuji, *Eur. J. Inorg. Chem.* **2016**, 607.
[15] M. Yoshifuji, T. Hashida, N. Inamoto, K. Hirotsu, T. Horiuchi, T. Higuchi, K. Ito, S. Nagase, *Angew. Chem. Int. Ed.* **1985**, *24*, 211.
[16] M. Yoshifuji, K. Shibayama, N. Inamoto, T. Matsushita, K. Nishimoto, *J. Am. Chem. Soc.* **1983**, *105*, 2495.
[17] A.-M. Caminade, M. Verrier, C. Ades, N. Paillous, M. Koenig, *J. Chem. Soc. Chem. Commun.* **1984**, 875.
[18] M. Yoshifuji, T. Sato, N. Inamoto, *Chem. Lett.* **1988**, *17*, 1735.
[19] P. Jutzi, U. Meyer, *J. Organomet. Chem.* **1987**, *333*, C18–C20.
[20] M. Yoshifuji, M. Abe, K. Toyota, K. Goto, N. Inamoto, *Bull. Chem. Soc. Jpn.* **1993**, *66*, 1572.
[21] K. Schwedtmann, M. H. Holthausen, C. H. Sala, F. Hennersdorf, R. Fröhlich, J. J. Weigand, *Chem. Commun.* **2016**, *52*, 1409.
[22] M. H. Holthausen, S. K. Surmiak, P. Jerabek, G. Frenking, J. J. Weigand, *Angew. Chem. Int. Ed.* **2013**, *52*, 11078.
[23] K. Schwedtmann, F. Hennersdorf, A. Bauzá, A. Frontera, R. Fischer, J. J. Weigand, *Angew. Chem. Int. Ed.* **2017**, *56*, 6218.
[24] G. Huttner, J. Borm, L. Zsolnai, *J. Organomet. Chem.* **1986**, *304*, 309.
[25] R. H. Crabtree, *The Organometallic Chemistry of the Transition Metals*, John Wiley & Sons, Inc, Hoboken, NJ, USA **2014**.
[26] K. Schwedtmann, J. Haberstroh, S. Roediger, A. Bauzá, A. Frontera, F. Hennersdorf, J. J. Weigand, *Chem. Sci.* **2019**, *10*, 6868.
[27] C. A. Tolman, *J. Am. Chem. Soc.* **1970**, *92*, 2953.

Manuscript received: May 15, 2023
Accepted manuscript online: September 6, 2023
Version of record online: September 6, 2023

Research Articles

Photoisomerization

C. Taube, J. Fidelius, K. Schwedtmann, C. Ziegler, F. Kreuter, L. Loots, L. J. Barbour, R. Tonner-Zech,* R. Wolf,* J. J. Weigand* **e202306706**

Visible-Light-Triggered Photoswitching of Diphosphene Complexes

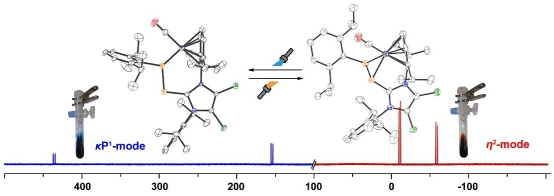

The photochemically and thermally reversible photoisomerization of η^2- to η^1-diphosphene complexes is described. The origins of this remarkable photochromic behavior lie in the S_1 excited state, as elucidated by theoretical studies. The findings underscore the potential of previously overlooked transition metal diphosphene complexes, revealing their promising photochromic properties and distinctive photoswitching behavior.